Effects of High Pressure on the Luminescence and Upconversion Properties of Ti^{2+}-Doped NaCl

Oliver S. Wenger, G. Mackay Salley, and Hans U. Güdel*

Departement für Chemie und Biochemie, Universität Bern, Freiestrasse 3, CH-3000 Bern 9, Switzerland

Received: May 8, 2002; In Final Form: July 12, 2002

The luminescence and upconversion properties of 0.8% Ti^{2+}-doped NaCl at 15 K are studied as a function of external hydrostatic pressure. Luminescence band maxima shifts are analyzed with a ligand field point charge model, allowing an estimate of the compressibility of the spectroscopically active $TiCl_6^{4-}$ unit in the NaCl host matrix. The pressure dependencies of the vibrational fine structures in the two Ti^{2+} luminescence bands are analyzed and interpreted in terms of pressure-induced changes in equilibrium distortions and force constants of the emitting electronic states $^3T_{2g}(t_{2g}e_g)$ and $^3T_{1g}(t_{2g}e_g)$. Time-resolved luminescence measurements are used to study the effects of pressure on the excited-state dynamics. 15 K near-infrared excitation at 9399 cm^{-1} leads to upconversion luminescence in the red spectral region both at ambient pressure and 34 kbar. On the basis of time-dependent upconversion luminescence experiments, two fundamentally different upconversion mechanisms are found to be dominant under these two experimental conditions. In particular, pressure is found to switch on an efficient upconversion mechanism, which is inactive at ambient pressure, leading to an estimated order-of-magnitude enhancement of the overall upconversion efficiency at 34 kbar. This additional mechanism involves energy transfer (ET) between two excited Ti^{2+} ions. Its occurrence only at high pressure is interpreted in terms of a strongly pressure-dependent spectral overlap integral governing the efficiency of the ET step.

I. Introduction

The aim of this paper is to explore the effect of pressure on the optical spectroscopic properties of Ti^{2+}-doped into a NaCl host matrix. At cryogenic temperatures, Ti^{2+} is a so-called dual emitter, i.e., it emits luminescence from two distinct excited states.[1,2] Among transition metal ions this is very unusual behavior, since in the vast majority of d-metal ions there is at most one such metastable excited state.[3] Among octahedrally coordinated transition metal ions Ti^{2+} is one of the few ions to exhibit upconversion phenomena.[4,5] This is because the existence of at least two metastable excited states is a fundamental prerequisite for upconversion processes.[6,7] In contrast to second-harmonic generation,[8] upconversion occurs via an intermediate metastable excited state which serves as an energy storage reservoir.[4] The upconversion luminescence is emitted from a higher excited state which is populated from this intermediate state either via radiative or nonradiative processes.[4] Recent studies on upconversion systems which involve transition metal ions have demonstrated that already subtle chemical and/or structural variations may lead to drastic changes in their upconversion properties and efficiencies.[9−11] This is because the spectroscopically active d-electrons have a large spatial extension, and thus strongly interact with their coordination environment. This has prompted us to study the effect of external hydrostatic pressure on the transition metal upconversion system Ti^{2+}:NaCl, to shine more light on this issue. The first preliminary results of our pressure studies on the upconversion processes in Ti^{2+}:NaCl and Ni^{2+}:$CsCdCl_3$ have been reported in refs 12 and 13.

Aside from its influence on the upconversion properties, we are interested in the effects of pressure on the excited-state dynamics and emission branching ratios, i.e., the interplay between radiative and nonradiative relaxation processes. With two long-lived metastable excited states the title system is ideally suited for that purpose. Finally, the Ti^{2+}:NaCl system shows some vibrational fine structure in its low-temperature absorption and luminescence bands.[2] This gives us the opportunity to obtain information about the pressure dependence of excited state distortions and force constants. These are issues which have been addressed only by rather few optical spectroscopic pressure studies published so far.

II. Experimental Section

The crystal growth is described in detail in ref 2. For all measurements a crystal with an estimated Ti^{2+} dopant concentration of 0.8 mol % was used.

The ambient pressure 15 K absorption spectrum was measured on a Cary 5e (Varian) instrument, and the sample was cooled in a closed-cycle He refrigerator (Air Products Displex).

Ambient pressure luminescence spectra were measured using a sample with the approximate dimensions 2 mm × 1 mm × 1 mm. Pressure-dependent luminescence spectra were obtained from a sample with a size of about 50 μm × 50 μm × 50 μm enclosed in a home-built sapphire anvil cell.[14] Berylco gaskets with a 300 μm diameter hole were used, and Merck spectroscopic paraffin oil served as pressure transmitting medium. The applied pressure was measured using the ruby R-line luminescence method.[15] Up to 34 kbar the ruby luminescence showed no significant broadening, indicating that the applied pressure stayed hydrostatic. Cooling of the whole pressure cell occurred in an appropriate home-built He gas flow cryostat.[14]

For continuous-wave luminescence spectroscopy the sample was excited with the 647.1 nm (15454 cm^{-1}) line of a Kr^+ laser (Coherent CR500K). Luminescence wavelength dispersion was achieved with a $^3/_4$ m single monochromator (Spex 1702) equipped with 600 grooves/mm gratings blazed at 750 nm.

10.1021/jp021140t CCC: $22.00
Published on Web 09/05/2002

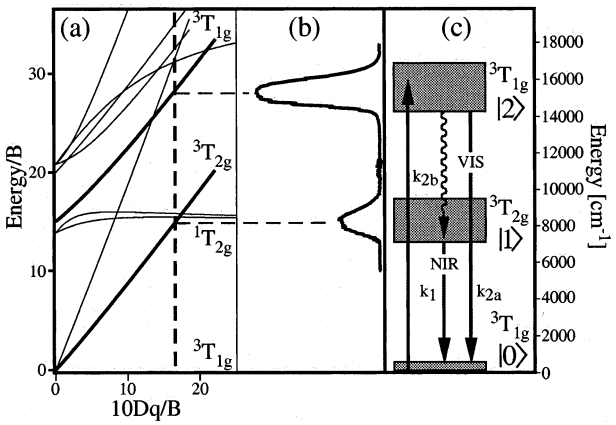

Figure 1. (a) Tanabe−Sugano energy level diagram for octahedrally coordinated d^2 ions. The dashed vertical line marks the $10Dq/B$ ratio for the ground-state geometry in Ti^{2+}:NaCl. (b) 15 K ambient pressure absorption spectrum of 0.8% Ti^{2+}:NaCl on a vertical energy axis. (c) Schematic energy level diagram for Ti^{2+}:NaCl including the ground state and its two metastable excited states. The solid upward arrow represents an absorption process, and the solid downward arrows stand for luminescence transitions. The wavy arrow represents nonradiative multiphonon relaxation.

Detection occurred with a cooled photomultiplier tube (RCA C31034) connected to a photon counting system (Stanford Research 400) in the case of $^3T_{1g}(t_{2g}e_g) \rightarrow {}^3T_{1g}(t_{2g}^2)$ luminescence, and with a liquid nitrogen cooled germanium detector (ADC 403L) or dry ice cooled lead sulfide detector (Hamamatsu P3337) connected to a lock-in amplifier (Stanford Research 830) in the case of $^3T_{2g}(t_{2g}e_g) \rightarrow {}^3T_{1g}(t_{2g}^2)$ luminescence. Survey luminescence spectra over the whole spectral range were recorded using the PbS detector.

For the luminescence decay measurements the sample was excited with a frequency doubled pulsed Nd^{3+}:YAG laser (Quanta Ray DCR-3, 20 Hz) pumped dye laser (Lambda Physik FL3002, DCM in methanol). The decay of the visible luminescence was detected as described above and recorded on a multichannel scaler (Stanford Research 430). The decay of the near-infrared luminescence was detected with a fast-response germanium detector (ADC 403HS) and recorded on an oscilloscope (Tektronix TDS540A).

Upconversion luminescence and transient measurements were performed using the fundamental of a pulsed Nd^{3+}:YAG laser (see above). Detection occurred as described above.

All luminescence spectra were corrected for the wavelength dependence of the sensitivity of the detection systems and converted to photon counts versus wavenumber following the procedure described in ref 16.

III. Results

Figure 1b shows the 15 K ambient pressure survey absorption spectrum of 0.8% Ti^{2+}:NaCl on a vertical energy axis. The two absorption bands are due to Ti^{2+} $^3T_{1g}(t_{2g}^2) \rightarrow {}^3T_{2g}(t_{2g}e_g)$ and $^3T_{1g}(t_{2g}^2) \rightarrow {}^3T_{1g}(t_{2g}e_g)$ transitions and have oscillator strengths of about 1.2×10^{-5} and 5×10^{-5}, respectively.

Figure 2 exhibits pressure-dependent 15 K survey luminescence spectra of Ti^{2+}:NaCl excited at 15454 cm^{-1}. Each spectrum consists of two broad luminescence bands: one located in the visible and one located in the near-infrared spectral range. With increasing pressure both shift to higher energies, while their relative integrated intensities stay constant within experimental accuracy.

In Figure 3 we present 15 K high resolution $^3T_{1g}(t_{2g}e_g) \rightarrow {}^3T_{1g}(t_{2g}^2)$ luminescence spectra at (a) ambient pressure, (b) 18 kbar, and (c) 34 kbar. In each spectrum a vibrational progression is observed. The energetic separation between individual progression members increases with pressure.

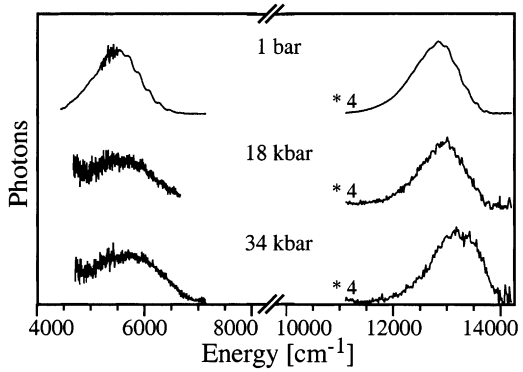

Figure 2. Variable pressure 15 K survey luminescence spectra obtained after excitation of 0.8% Ti^{2+}:NaCl at 15454 cm^{-1}. The intensity of the higher energy luminescence band has been scaled up by a factor of 4 relative to the lower energy band.

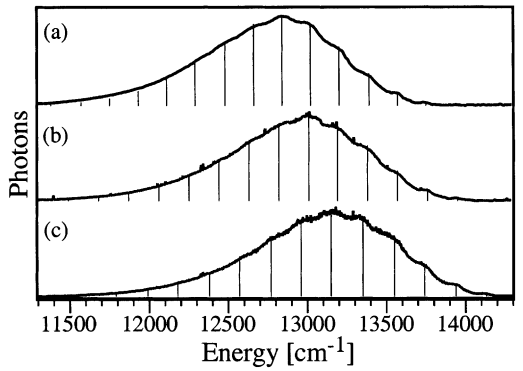

Figure 3. 15 K high-resolution $^3T_{1g}(t_{2g}e_g) \rightarrow {}^3T_{1g}(t_{2g}^2)$ luminescence spectra at (a) ambient pressure, (b) 18 kbar, and (c) 34 kbar. Excitation occurred at 15454 cm^{-1} for all spectra. The vertical bars represent the best fits with eq 3 to the experimental data.

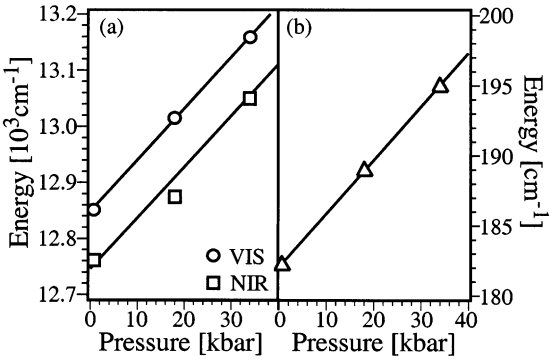

Figure 4. (a) Energy of the $^3T_{1g}(t_{2g}e_g) \rightarrow {}^3T_{1g}(t_{2g}^2)$ (circles) and $^3T_{2g}(t_{2g}e_g) \rightarrow {}^3T_{1g}(t_{2g}^2)$ (squares) luminescence band maxima as a function of external pressure. The latter data points were arbitrarily shifted to higher energies by 7300 cm^{-1}. The straight lines are linear regression fits to the experimental data with slopes of 9 cm^{-1}/kbar. (b) Vibrational energy of the progression mode in the $^3T_{1g}(t_{2g}e_g) \rightarrow {}^3T_{1g}(t_{2g}^2)$ and $^3T_{2g}(t_{2g}e_g) \rightarrow {}^3T_{1g}(t_{2g}^2)$ luminescence bands as a function of pressure (triangles). The straight line is a fit to these data yielding a slope of 0.4 cm^{-1}/kbar.

In Figure 4a the band maximum energies of the visible ("VIS", circles) and near-infrared ("NIR", squares) luminescences from Figure 2 are plotted as a function of pressure. The NIR data points have been arbitrarily shifted to higher energies by 7300 cm^{-1}. Simple Gaussian-type functions were fitted to the experimental spectra in order to determine the band

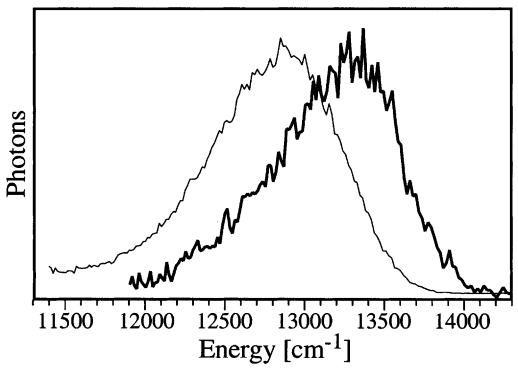

Figure 5. 15 K upconversion luminescence spectra obtained after pulsed excitation of 0.8% Ti^{2+}:NaCl at 9399 cm^{-1} for ambient pressure (faint line) and 34 kbar (strong line).

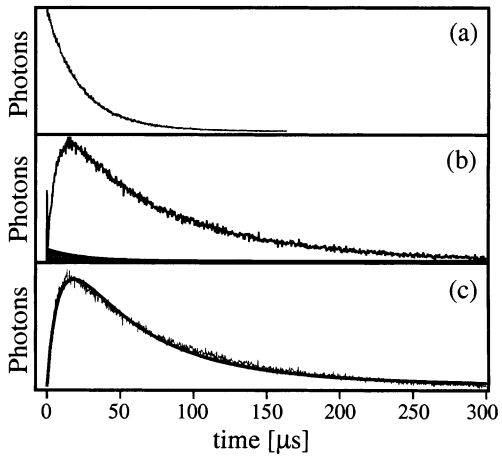

Figure 6. Temporal evolution of the 15 K upconversion luminescence intensity after 10 ns pulsed excitation at 9399 cm^{-1} for (a) ambient pressure and (b) 34 kbar. (c) is the same transient as (b) after subtraction of the GSA/ESA upconversion contribution, i.e., the shaded area in Figure 6b. The solid line is a fit to the experimental data with eq 6, and the fit parameters are given in Table 4.

TABLE 1: 15 K Lifetimes τ of the Two Metastable Excited States in 0.8% Ti^{2+}:NaCl at Ambient Pressure and 34 kbar

excited state	τ (1 bar)	τ (34 kbar)
$^3T_{2g}(t_{2g}e_g)$	(1.5 ± 0.1) ms	(1.5 ± 0.8) ms
$^3T_{1g}(t_{2g}e_g)$	(23 ± 1) μs	(22 ± 4) μs

maximum energies. The error on these energies is ± 5 cm^{-1} for the VIS and ± 10 cm^{-1} for the NIR data points. Linear regression fits to both data sets are included in Figure 4, and they both yield a slope of 9 cm^{-1}/kbar, i.e., the two luminescence band maximum energies have an equal pressure dependence. Figure 4b exhibits the vibrational energy of the progression mode in the $^3T_{1g}(t_{2g}e_g) \rightarrow {}^3T_{1g}(t_{2g}^2)$ and $^3T_{2g}(t_{2g}e_g) \rightarrow {}^3T_{1g}(t_{2g}^2)$ luminescence bands as a function of pressure (triangles). The solid line is a linear regression fit to these data with a slope of 0.4 cm^{-1}/kbar.

Table 1 lists the 15 K lifetimes of $^3T_{2g}(t_{2g}e_g)$ and $^3T_{1g}(t_{2g}e_g)$ at ambient pressure and 34 kbar. The respective luminescence decays are shown in Figure S1 of the supporting material. At 34 kbar, both the $^3T_{2g}(t_{2g}e_g)$ and the $^3T_{1g}(t_{2g}e_g)$ population decays are not purely single exponential. This is attributed to small inhomogeneities in the applied pressure.

Figure 5 shows the 15 K ambient pressure (faint line) and 34 kbar (strong line) upconversion luminescence spectra obtained after excitation at 9399 cm^{-1}. There is a blue-shift of the luminescence with pressure. This shift is identical to the shift of the $^3T_{1g}(t_{2g}e_g) \rightarrow {}^3T_{1g}(t_{2g}^2)$ luminescence band obtained after direct $^3T_{1g}(t_{2g}e_g)$ excitation at 15454 cm^{-1}; see Figure 3.

The temporal evolution of the 15 K upconversion luminescence after 10 ns excitation pulses at 9399 cm^{-1} is shown in Figure 6. At ambient pressure (a) there is an instantaneous decay. At 34 kbar (b) there is a rise preceding the decay. The rise time in (b) is on the order of a few microseconds, and thus close to the $^3T_{1g}(t_{2g}e_g)$ upper level lifetime. The decay time is around 80 μs and thus about a factor of 4 longer than the inherent upper level lifetime; see above, but still substantially shorter than the $^3T_{2g}(t_{2g}e_g)$ intermediate level lifetime.

IV. Discussion

A. Ambient Pressure Absorption and Luminescence Properties of Ti^{2+}:NaCl. In NaCl the Ti^{2+} dopant ion is octahedrally coordinated by six chloride anions.[2] The 15 K ambient pressure absorption spectrum of 0.8% Ti^{2+}-doped NaCl presented in Figure 1b shows the typical features of octahedrally coordinated d^2 ions.[17] Two broad bands centered around 8170 and 15230 cm^{-1} with oscillator strengths on the order of 10^{-5} are observed. According to the d^2 Tanabe-Sugano energy level diagram in Figure 1a,[18] their assignment to the $^3T_{1g}(t_{2g}^2) \rightarrow {}^3T_{2g}(t_{2g}e_g)$ and $^3T_{1g}(t_{2g}^2) \rightarrow {}^3T_{1g}(t_{2g}e_g)$ transitions is straightforward. This is emphasized by the dashed horizontal lines in Figure 1a,b. Both transitions are spin-allowed and involve an electron promotion from a weakly antibonding t_{2g} to a stronger antibonding e_g orbital. As a consequence the $TiCl_6^{4-}$ complex undergoes an overall expansion upon photoexcitation to these states, and this causes the absorption bands to be broad.[19] No spin-forbidden absorption transitions are observed: these are particularly weak in Ti^{2+} due to its low spin−orbit coupling.[20] A fit of calculated to experimental excited-state energies yields the ligand field parameters $10Dq = 9064$ cm^{-1}, $B = 530$ cm^{-1}, and $C/B = 3.76$.[2] Thus, as illustrated by the vertical dashed line in Figure 1a, for Ti^{2+}:NaCl $10Dq/B = 17.1$. Consequently, $^3T_{2g}(t_{2g}e_g)$ is the lowest energetic excited state in this system at ambient pressure. This is in contrast to Ti^{2+}:$MgCl_2$, in which the ligand field strength is such that $^1T_{2g}(t_{2g}^2)$ lies below $^3T_{2g}(t_{2g}e_g)$.[21,22]

Laser excitation into $^3T_{1g}(t_{2g}e_g)$ at 15 K and ambient pressure leads to the luminescence spectrum shown at the top of Figure 2. According to their energies, bandwidths and their different decay behavior, the two bands have been assigned to $^3T_{2g}(t_{2g}e_g) \rightarrow {}^3T_{1g}(t_{2g}^2)$ and $^3T_{1g}(t_{2g}e_g) \rightarrow {}^3T_{1g}(t_{2g}^2)$ luminescence,[2] i.e., to the reverse transitions of those in Figure 1b. This is schematically illustrated by the solid downward arrows labeled "NIR" and "VIS" in the simplified energy level diagram of Figure 1c. $^3T_{2g}(t_{2g}e_g)$ is populated via nonradiative relaxation from $^3T_{1g}(t_{2g}e_g)$; see the wavy arrow. A radiative $^3T_{1g}(t_{2g}e_g) \rightarrow {}^3T_{2g}(t_{2g}e_g)$ transition is not observed due to its weakness.[2,1]

B. Effect of Pressure on the Luminescence Band Maximum Energies: Analysis with a Ligand Field Point Charge Model. Upon application of external hydrostatic pressure both the $^3T_{2g}(t_{2g}e_g) \rightarrow {}^3T_{1g}(t_{2g}^2)$ and the $^3T_{1g}(t_{2g}e_g) \rightarrow {}^3T_{1g}(t_{2g}^2)$ luminescence band undergo a blue-shift; see Figure 2. This is because the energies of both emitting excited states are strongly ligand field dependent; see the Tanabe−Sugano energy level diagram of Figure 1a: In the strong-field limit the energies of the $^3T_{2g}(t_{2g}e_g)$ and $^3T_{1g}(t_{2g}e_g)$ states have a linear dependence on the octahedral ligand field parameter $10Dq$, which is a direct measure for the $t_{2g}-e_g$ splitting.[19] The pressure-induced changes in $10Dq$ and the Racah B parameter can be quantified with a simple ligand field calculation.[18] The result of this calculation is shown in Table 2. External pressure leads to an increase of

TABLE 2: Ligand Field Parameters for the Relaxed $^3T_{2g}(t_{2g}e_g)$ and $^3T_{1g}(t_{2g}e_g)$ Excited States of Ti^{2+} in NaCl at 15 K as a Function of External Hydrostatic Pressure

pressure [kbar]	$10Dq$ [cm^{-1}]	B [cm^{-1}]
10^{-3}	6202	542
18	6354	544
34	6525	544

$10Dq$ with a rate of roughly 9 cm^{-1}/kbar, whereas B essentially stays constant. This indicates that in the 1 bar−34 kbar range the interelectronic repulsion is not affected by external pressure, or in other words, the covalency of the $Ti^{2+}-Cl^-$ interaction remains unchanged. Note that since we calculate $10Dq$ and B on the basis of luminescence data, these crystal field parameters are valid for the relaxed $^3T_{2g}(t_{2g}e_g)$ and $^3T_{1g}(t_{2g}e_g)$ excited states and not for the $^3T_{1g}(t_{2g}^2)$ ground state such as in section IV.A.

From the pressure dependence of $10Dq$ we can extract information about the local compressibility χ_{loc} of the optically active $TiCl_6^{4-}$ unit. For that purpose we make use of a simple point charge model, a common approach to estimate χ_{loc} in transition metal complexes.[23,24] In this model $10Dq$ is proportional to R^{-5} where R is the metal (Ti^{2+})−ligand (Cl^-) distance. It follows that $10Dq$ is proportional to $V^{-5/3}$, where V is the volume of the octahedral $TiCl_6^{4-}$ unit. Consequently,

$$\ln\left(\frac{10Dq}{10Dq_0}\right) = -\frac{5}{3}\ln\left(\frac{V}{V_0}\right) + \text{constant} \qquad (1)$$

where the zero subscripts denote ambient pressure quantities. The compressibility χ is a measure of the energy required to produce a given deformation. Therefore it is defined as[25]

$$\chi = -\frac{1}{V}\left(\frac{dV}{dP}\right)_T = -\frac{d\ln(V)}{dP} \qquad (2)$$

Figure 7 shows a plot of $\ln(V/V_0)$ versus pressure (open circles). These values were calculated with eq 1 from the $10Dq$ values in Table 2. The solid line through these data points is a linear regression fit with a slope of -9×10^{-4} $kbar^{-1}$. Its absolute value corresponds to the local compressibility χ_{loc} of the $TiCl_6^{4-}$ unit is NaCl at 15 K; see eq 2. The faint line illustrates the literature value of the bulk compressibility of the NaCl host material at 15 K as a function of pressure. It has a slope of $-\chi_{bulk} = -3.8 \times 10^{-3}$ $kbar^{-1}$.[26,27] This illustrates that the local compressibility at the $TiCl_6^{4-}$ dopant site is roughly a factor of 4 lower than the compressibility of the NaCl host material. Several previous pressure studies on transition-metal-doped inorganic systems have focused on the differences between the local compressibility of the optically active unit and the bulk compressibility of the host.[23,28] Often, the conclusion was reached that the basic assumption of the point charge model, namely, that $10Dq \propto R^{-n}$ with $n = 5$, is slightly incorrect, and consequently n was estimated to adopt values between 4.5 and 6, depending on the system.[29−31] Other studies relate the differences between χ_{loc} and χ_{bulk} to size differences between dopant ion and substituted host ions.[28] None of these two explanations alone can satisfactorily account for the factor of 4 difference between χ_{loc} and χ_{bulk} in Ti^{2+}:NaCl. In this system Ti^{2+} substitutes for Na^+. This requires a charge compensation which very likely occurs as a Na^+ vacancy.[2] For electrostatic reasons the Ti^{2+} dopant ion and the Na^+ vacancy are most likely in immediate neighborhood. We conclude that this has a significant influence on the effect of pressure on the optically active $TiCl_6^{4-}$ complex. In particular, the effect of the external pressure in the Ti^{2+} environment is potentially taken up by the Na^+ vacancy. Thus the pressure dependence of $10Dq$ in Ti^{2+}:NaCl is unusually low for a 3d-metal-doped chloride system,[23] and this is the manifestation of the low χ_{loc} value compared to χ_{bulk}.

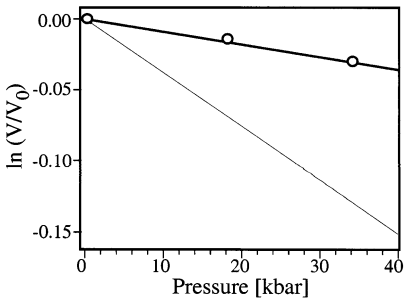

Figure 7. Semilogarithmic plot of the volume compression V/V_0 of the $TiCl_6^{4-}$ unit in NaCl at 15 K as a function of external pressure. The open circles correspond to the experimentally achieved pressures, and the $\ln(V/V_0)$ values were calculated with eq 1 using the $10Dq$ values given in Table 2. The bold line is a linear regression fit to these data with a slope of $-\chi_{loc} = 9 \times 10^{-4}$ $kbar^{-1}$; see eq 2. The faint line is the expected volume compression on the basis of the 15 K NaCl bulk compressibility, i.e., for $\chi_{bulk} = -3.8 \times 10^{-3}$ $kbar^{-1}$.

C. Pressure Effect on Potential Energy Surfaces and Excited-state Lifetimes. Figure 3 shows the pressure-dependent 15 K $^3T_{1g}(t_{2g}e_g) \rightarrow {}^3T_{1g}(t_{2g}^2)$ luminescence band in high resolution. In each spectrum a vibrational progression is observed. The energetic separation between the individual progression members increases from (a) 182 cm^{-1} at ambient pressure to (b) 189 cm^{-1} at 18 kbar and (c) 195 cm^{-1} at 34 kbar; see the triangles in Figure 4b. Analogous vibrational progressions with an identical pressure dependence have been observed in high-resolution spectra of the high-energy side of the $^3T_{2g}(t_{2g}e_g) \rightarrow {}^3T_{1g}(t_{2g}^2)$ luminescence band (data not shown). In a previous ambient pressure study of Ti^{2+}:NaCl this progression has been identified as mainly due to an e_g-vibration, and it is a manifestation of the fact that the $^3T_{1g}(t_{2g}e_g)$ and $^3T_{2g}(t_{2g}e_g)$ potentials are displaced along the e_g normal coordinate relative to the $^3T_{1g}(t_{2g}^2)$ ground state.[2] Although no a_{1g} progressions ($\nu_{a1g} \approx 250$ cm^{-1} [2]) are directly observable in our absorption and luminescence spectra, it does not necessarily follow that the a_{1g} displacement of the $^3T_{2g}(t_{2g}e_g)/{}^3T_{1g}(t_{2g}e_g)$ excited-state potentials on one hand and the $^3T_{1g}(t_{2g}^2)$ ground-state potential on the other hand is zero; see, for example refs 32 and 33. However, on the basis of our experimental data, it appears reasonable to assume that the e_g displacement is dominant. Since we are dealing with emission data, we are probing the pressure dependence of the e_g vibrational energy $\bar{\nu}_{e_g}$ in the ground state. A linear regression fit to the data in Figure 4b (solid line) yields a slope of $\Delta\bar{\nu}_{e_g} = 0.4$ cm^{-1}/kbar. This compares to pressure-induced shift rates for e_g vibrational energies of $\Delta\bar{\nu}_{e_g} = 0.55$ cm^{-1}/kbar for $CrCl_6^{3-}$ in $Cs_2NaScCl_6$ and $\Delta\bar{\nu}_{e_g} = 1.1$ cm^{-1}/kbar for CrF_6^{3-} in K_2NaScF_6.[34,35] Thus, the slightly lower value for $\Delta\bar{\nu}_{e_g}$ in our system reflects the relatively low effect pressure has on the $TiCl_6^{4-}$ in NaCl, i.e., this is in line with the low χ_{loc} value discussed above.

For Franck−Condon transitions at the lowest temperatures emission band shapes can be calculated with[36]

$$I_n = \frac{e^{-S}S^n}{n!} \qquad (3)$$

where I_n is the intensity of the nth member of the vibrational progression and S is the so-called Huang−Rhys parameter. The vertical bars in Figure 3 represent the best fits with eq 3 to the

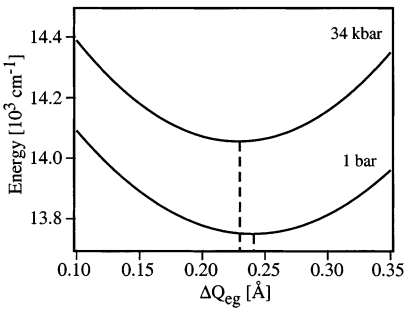

Figure 8. Single configurational coordinate (SCC) diagram showing the $^3T_{1g}(t_{2g}e_g)$ excited-state potential at ambient pressure and 34 kbar for the e_g normal coordinate. The zero point of this SCC plot corresponds to the $^3T_{1g}(t_{2g}^2)$ ground-state potential minimum.

TABLE 3: Summary of the Parameters Extracted from the Data in Figures 3 and 4b: Vibrational Energy $\bar{\nu}_{e_g}$, Force Constant f_{e_g}, Huang−Rhys Parameter S_{e_g} and Equilibrium Displacement $|\Delta Q_{e_g}|_{eq}$ of the $^3T_{1g}(t_{2g}e_g)$ Excited State Potential Relative to the $^3T_{1g}(t_{2g}^2)$ Ground State Potential along the e_g Normal Coordinate as a Function of the Applied Pressure

p [kbar]	$\bar{\nu}_{e_g}$ [cm^{-1}]	f_{e_g} [N/m]	S_{e_g}	$\lvert\Delta Q_{e_g}\rvert_{eq}$ [Å]
10^{-3}	182	69.3	5.5	0.240
18	189	74.7	5.5	0.235
34	195	79.5	5.4	0.229

experimental data. They yield $S_{e_g} = 5.5$ at 1 bar as well as at 18 kbar and $S_{e_g} = 5.4$ at 34 kbar; see Table 3. In a simple linear harmonic coupling picture this Huang−Rhys parameter characterizes the relative equilibrium displacement $|\Delta Q|_{eq}$ of two potentials.[36] Table 3 summarizes the calculated $|\Delta Q_{e_g}|_{eq}$ values for the three experimentally achieved pressures: the equilibrium displacement between the $^3T_{1g}(t_{2g}^2)$ and $^3T_{1g}(t_{2g}e_g)$ potentials decreases with pressure from 0.240 Å at ambient pressure to 0.235 Å at 18 kbar and 0.229 Å at 34 kbar. Note that these numbers represent upper limits for the actual e_g distortions. As mentioned above, there is a possibility of a small but nonzero a_{1g} distortion in our system, which has been neglected in the foregoing analysis. The reduction of $|\Delta Q_{e_g}|_{eq}$ reflects the fact that with increasing pressure the expansion of the $TiCl_6^{4-}$ unit upon photoexcitation into $^3T_{1g}(t_{2g}e_g)$ becomes inhibited. The single configurational coordinate (SCC) diagram in Figure 8 summarizes the findings of this and the previous section. It shows the $^3T_{1g}(t_{2g}e_g)$ potential at 1 bar and at 34 kbar. The zero-point of this SCC plot corresponds to the $^3T_{1g}(t_{2g}^2)$ ground-state potential minimum. The three main effects of external pressure are illustrated in this diagram: The excited-state potential minimum energy is increased with respect to the ground state, the equilibrium displacement relative to the ground-state potential is decreased and the force constant is increased (in order of decreasing importance).

Table 1 and Figure S1 of the supporting material show that the 15 K lifetimes of both metastable excited states stay essentially constant between ambient pressure and 34 kbar. This is explained as follows: At 15 K and ambient pressure $^3T_{2g}(t_{2g}e_g)$ depopulation occurs entirely radiatively.[2] With increasing pressure the energy of $^3T_{2g}(t_{2g}e_g)$ relative to the ground state increases; see section IV.B, while the displacement of the potentials decreases; see section IV.C. Both effects are in favor of radiative $^3T_{2g}(t_{2g}e_g)$ emission,[36] and thus the 15 K $^3T_{2g}(t_{2g}e_g)$ lifetime stays radiative and essentially constant between 1 bar and 34 kbar.

The dominant 15 K $^3T_{1g}(t_{2g}e_g)$ depopulation mechanism at ambient pressure is nonradiative multiphonon relaxation to $^3T_{2g}(t_{2g}e_g)$.[2] The $^3T_{1g}(t_{2g}e_g)$ and $^3T_{2g}(t_{2g}e_g)$ potentials have a very similar pressure dependence regarding their energy shifts (section IV.B), their equilibrium displacements, and their force constants (section IV.C). Thus, for the two potentials relative to each other, all these parameters remain essentially unchanged with pressure. Consequently, $^3T_{1g}(t_{2g}e_g) \rightsquigarrow {}^3T_{2g}(t_{2g}e_g)$ multiphonon relaxation and thus the 15 K lifetime of $^3T_{1g}(t_{2g}e_g)$ is not affected by pressure in the 1 bar−34 kbar range.

D. Upconversion. *1. General Considerations.* Since the first report of upconversion more than 40 years ago,[37] several mechanisms by which this nonlinear optical process can occur have been established.[38] Before identifying those which are active in Ti^{2+}-doped NaCl, we first very briefly summarize the two most relevant ones.

(a) GSA/ESA. This mechanism involves two radiative absorption steps. Ground state absorption (GSA) promotes the upconversion system to its intermediate metastable excited state. From there, excited state absorption (ESA) to the upper emitting state can occur. Since both steps are radiative, this mechanism can only take place while the system is irradiated with excitation light.

(b) GSA/ETU. In this mechanism two ions excited to their intermediate excited states by GSA combine their energy nonradiatively to produce one ion in the upper emitting state and another ion in the ground state. The second step is called energy transfer upconversion (ETU). Once the system has been excited to its intermediate metastable state, this process can proceed for a time related to the lifetime of the intermediate level even in the absence of further light irradiation.

2. Influence of External Pressure on the Upconversion Mechanisms Active in Ti^{2+} Doped NaCl. The temporal evolution of the upconversion spectra in Figure 5 after 10 ns near-IR excitation pulses are shown in Figure 6a,b. These transients can be used as diagnostics for the identification of the upconversion mechanisms.[4] At ambient pressure (Figure 6a) an instantaneous decay of the upconversion luminescence is observed with a decay time of 22 μs, which corresponds to the $^3T_{1g}(t_{2g}e_g)$ lifetime; see Table 1. This is typical behavior for a pure GSA/ESA mechanism.[4,39] At 34 kbar, the upconversion transient is comprised of a slow rise preceding the decay. This is typical behavior for a GSA/ETU mechanism.[4,40] Inspection of Figure 6b shows that there is a small but significant nonzero luminescence intensity at $t = 0$, i.e., immediately after the laser pulse. This is due to a small fraction of GSA/ESA excitation. However, as emphasized by the shaded area in Figure 6b, only about 5% of the total upconversion luminescence intensity after the excitation pulse is due to this mechanism. This indicates that at 34 kbar the GSA/ETU mechanism is 20 times more efficient than GSA/ESA. We conclude that external pressure induces a change from an exclusive GSA/ESA mechanism at 1 bar to a dominant GSA/ETU mechanism at 34 kbar. To explain this behavior, we first have to identify the involved GSA, ESA, and ETU processes in Ti^{2+}:NaCl.

GSA at 9399 cm^{-1} occurs into the high-energy side of the $^3T_{2g}(t_{2g}e_g)$ absorption band; see Figure 1b and the Ti^{2+} energy level schemes in Figure 9. This is followed by rapid nonradiative relaxation to the $^3T_{2g}(t_{2g}e_g)$ potential minimum at about 6750 cm^{-1}. From there, ESA to the $^3T_{1g}(t_{2g}e_g)$ state can occur; see Figure 9a. For the ETU process illustrated in Figure 9b two Ti^{2+} ions have to be excited to $^3T_{2g}(t_{2g}e_g)$. The energy transfer process itself can only occur, if there is a nonzero spectral overlap of the donor emission profile with the acceptor absorption profile.[41,42] In our specific case the two relevant profiles are those of $^3T_{2g}(t_{2g}e_g) \rightarrow {}^3T_{1g}(t_{2g}^2)$ emission and $^3T_{2g}(t_{2g}e_g) \rightarrow {}^3T_{1g}(t_{2g}e_g)$ ESA. There is no direct information about the latter

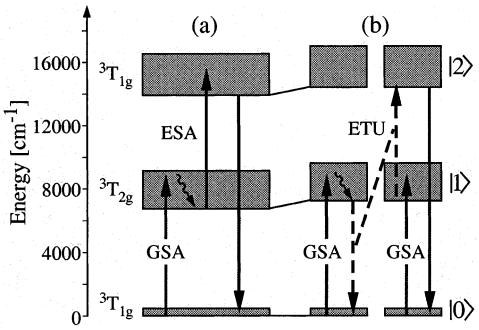

Figure 9. Energy level schemes for Ti^{2+}:NaCl illustrating the dominant upconversion mechanisms at (a) ambient pressure and (b) 34 kbar. The solid upward arrows represent the radiative processes of ground-state absorption (GSA) and excited-state absorption (ESA). The solid downward arrows stand for luminescence transitions. The dashed arrows represent a nonradiative energy transfer upconversion (ETU) process, and the wavy downward arrows represent multiphonon relaxation.

available. However, for energetic reasons it is expected to have its onset at about 7000 cm^{-1}, i.e., at the energy difference between the $^3T_{2g}(t_{2g}e_g)$ and $^3T_{1g}(t_{2g}e_g)$ potential minima.[9] As discussed in sections IV.B and IV.C, these two potentials have an essentially equal pressure dependence, and in particular their pressure-induced energy shift rates are identical up to 34 kbar; see Figure 4a. In Figure 9 this is illustrated by the parallel lines connecting schemes (a) and (b). Thus $^3T_{2g}(t_{2g}e_g) \rightarrow {}^3T_{1g}(t_{2g}e_g)$ ESA is expected to be essentially pressure-independent. At ambient pressure and 15 K $^3T_{2g}(t_{2g}e_g) \rightarrow {}^3T_{1g}(t_{2g}^2)$ emission extends from 6750 cm^{-1} to about 4400 cm^{-1}; see Figure 2 (top). Consequently, under these conditions there is no spectral overlap with the above ESA transition, and thus ETU does not take place. At 34 kbar and 15 K $^3T_{2g}(t_{2g}e_g) \rightarrow {}^3T_{1g}(t_{2g}^2)$ emission has its onset at about 7050 cm^{-1}, Figure 2 (bottom), and consequently there is some spectral overlap with $^3T_{2g}(t_{2g}e_g) \rightarrow {}^3T_{1g}(t_{2g}e_g)$ ESA, which activates the ETU mechanism.

Based on the upconversion transients presented in Figure 6a/b we can make an estimate on the relative efficiencies of the upconversion processes at ambient pressure and 34 kbar. For a GSA/ESA upconversion mechanism the population density N_2 of the upper emitting state $|2\rangle$, in our case $^3T_{1g}(t_{2g}e_g)$ (see Figure 9), is proportional to the product $\sigma_{GSA}\sigma_{ESA}$ of the GSA and ESA cross sections at the excitation wavelength:[4,43]

$$N_2 \propto P^2\sigma_{GSA}\sigma_{ESA}N_0 \qquad (4)$$

with N_0 the ground-state population density and P the laser power. Similarly, for a GSA/ETU mechanism the following relation is valid:[4,43]

$$N_2 \propto P^2\omega_{ETU}{\sigma_{GSA}}^2{N_0}^2 \qquad (5)$$

with ω_{ETU} the power-independent ETU rate parameter.[4] We assume that σ_{ESA} stays constant between 1 bar and 34 kbar, and this is justified by the pressure independence of the upconversion relevant ESA transition; see above. On the basis of the 15 K ambient pressure GSA spectrum in Figure 1b and the $^3T_{2g}(t_{2g}e_g)$ shift rate of 9 cm^{-1}/kbar, we estimate that at 9399 cm^{-1} σ_{GSA} increases by a factor of 2 between 1 bar and 34 kbar. Consequently, in this pressure range and for 9399 cm^{-1} excitation the efficiency of the GSA/ESA mechanism is expected to double. Nevertheless, as discussed above, the transient in Figure 6b shows that at 34 kbar GSA/ETU is 10 times more efficient than GSA/ESA. This is because the ETU rate parameter ω_{ETU} has increased from zero to a finite value; see above. Thus we conclude that in our experiment the overall upconversion efficiency has increased by about a factor of 20 between ambient pressure and 34 kbar.

TABLE 4: Kinetic Parameters for 0.8% Ti^{2+}:NaCl Used in Equation 6 to Simulate the 15 K, 34 kbar Upconversion Transient in Figure 6c

electronic transition	label (Figure 1c, eq 6)	rate constant value (s^{-1})
$^3T_{1g}(t_{2g}e_g) \rightarrow {}^3T_{1g}(t_{2g}^2)$	k_{2a}	8696
$^3T_{1g}(t_{2g}e_g) \rightsquigarrow {}^3T_{2g}(t_{2g}e_g)$	k_{2b}	34872
$^3T_{2g}(t_{2g}e_g) \rightarrow {}^3T_{1g}(t_{2g}^2)$	k_1	667
ETU rate constant	$\omega_{ETU}N_1$	38000

3. Kinetic ETU Model. Figure 6c shows the 15 K, 34 kbar upconversion transient from Figure 6b after subtraction of the GSA/ESA contribution (shaded area), i.e., this transient reflects the dynamics of the pure GSA/ETU mechanism. We use the set of coupled nonlinear rate equations presented in eq 6 to simulate these data:

$$\begin{aligned} dN_0/dt &= -GN_0 + k_1N_1 + k_{2a}N_2 + \omega_{ETU}{N_1}^2 \\ dN_1/dt &= GN_0 - k_1N_1 + k_{2b}N_2 - 2\omega_{ETU}{N_1}^2 \\ dN_2/dt &= -(k_{2a} + k_{2b})N_2 + \omega_{ETU}{N_1}^2 \end{aligned} \qquad (6)$$

where G is the GSA rate constant and N_0, N_1, and N_2 correspond to the excitation densities (ions/cm^3) of the $^3T_{1g}(t_{2g}^2)$, $^3T_{2g}(t_{2g}e_g)$, and $^3T_{1g}(t_{2g}e_g)$ electronic levels, respectively. ω_{ETU} (cm^3 s^{-1}) is the effective rate parameter governing ETU. The rate constants k_1, k_{2a}, and k_{2b} (s^{-1}) represent (radiative and nonradiative) relaxation processes from the two metastable excited states, and they are defined in Figure 1c and Table 4. k_1 and $(k_{2a} + k_{2b})$ are the inverse of the 15 K $^3T_{2g}(t_{2g}e_g)$ and $^3T_{1g}(t_{2g}e_g)$ lifetimes, respectively, and as such they are experimentally accessible; see Table 1. The decay from $^3T_{2g}(t_{2g}e_g)$ is entirely radiative; see section IV.C. Consequently, the ratio k_{2a}/k_{2b} can be determined from the survey luminescence spectra in Figure 2: It corresponds to the ratio of the total number of photons emitted in $^3T_{1g}(t_{2g}e_g) \rightarrow {}^3T_{1g}(t_{2g}^2)$ to the total number of photons emitted in $^3T_{2g}(t_{2g}e_g) \rightarrow {}^3T_{1g}(t_{2g}^2)$, and thus we find $k_{2a}/k_{2b} = 1{:}4$. Thus we obtain the rate constant values summarized in Table 4. We use $\omega_{ETU}N_1$, i.e., the ETU rate constant as the only adjustable parameter in eq 6 to simulate the transient in Figure 6c. The result of the best fit is obtained with $\omega_{ETU}N_1 = 38000$ s^{-1}, and is included in Figure 6c (solid line). In view of the simplicity of our model and the fact that a single fit parameter is used, its agreement with experiment is very good. From our modeling we are able to relate the rise of the upconversion transient to the decay of the upper level and associate the decay part of the transient with the decay of the intermediate level. Both of these values are slightly modified by the large $\omega_{ETU}N_1$ rate constant.

This high $\omega_{ETU}N_1$ value implies that the Ti^{2+} ions which participate in the ETU process have a very short intermediate level lifetime, i.e., $(\omega_{ETU}N_1 + k_1)^{-1} = 26$ μs. At first sight this appears to be in contradiction with the $^3T_{2g}(t_{2g}e_g)$ lifetime values in Table 1. Several previous upconversion studies have established that efficient ETU processes are essentially restricted to nearest neighbor ion pairs, i.e., to a very specific subset of the optically active dopant ions.[44,45] Assuming a homogeneous distribution of Ti^{2+} dopant ions in 0.8% Ti^{2+}:NaCl this subset consists of approximately 5% of all Ti^{2+} ions in this crystal. The bulk of Ti^{2+} ions, 95%, is ETU inactive and decays with $k_1^{-1} = 1.5$ ms; see Table 1.

Within the ETU active subset the upconversion branching ratio $(\omega_{ETU}N_1)/k_1 = 57$, i.e., for $^3T_{2g}(t_{2g}e_g)$ excited Ti^{2+} ions ETU to $^3T_{1g}(t_{2g}e_g)$ is 57 times faster than decay to the ground state. Only 20% of all $^3T_{1g}(t_{2g}e_g)$ excited Ti^{2+} ions emit in the visible; see above, and therefore the calculated $^3T_{1g}(t_{2g}e_g) \rightarrow {}^3T_{1g}(t_{2g}^2)$ ("VIS"): $^3T_{2g}(t_{2g}e_g) \rightarrow {}^3T_{1g}(t_{2g}^2)$ ("NIR") intensity ratio after pulsed $^3T_{1g}(t_{2g}e_g)$ excitation at 15 K and 34 kbar is 11:1 for the ETU subset alone, and 11:20 for the whole ensemble of Ti^{2+} ions, i.e., ETU subset and bulk ions together since the latter emit only in the NIR. After continuous-wave (cw) $^3T_{1g}(t_{2g}e_g)$ excitation[49] at ambient pressure and 15 K this ratio was found to be around 1:1000.[9] This value is determined from the integrated VIS luminescence and NIR luminescence under NIR excitation. Consequently, a pressure increase from 1 bar to 34 kbar increases the VIS:NIR luminescence ratio after pulsed $^3T_{2g}$-$(t_{2g}e_g)$ excitation at 15 K by a factor of 550, whereas from the upconversion transient data in Figure 6a,b an increase in the upconversion efficiency by a factor of 20 was estimated; see above. The order-of-magnitude discrepancy of these two estimates is attributed to differences in the near-infrared laser excitation power in the pulsed and cw-experiments. In the former the achieved peak power is substantially higher than the laser power used in the cw-measurement.

V. Conclusions

At cryogenic temperatures the Ti^{2+} ion exhibits very rich photophysics. Particularly regarding its luminescence properties, Ti^{2+} exhibits a behavior which is unusual among transition metal ions. Together with Ni^{2+}, it is the only ion known to date which, in octahedral coordination, exhibits luminescence from two strongly ligand-field-dependent excited states.[4] Thus, application of external hydrostatic pressure has a dramatic effect on the luminescence properties of these ions. Since two states emit luminescence, we obtain an unusually detailed picture of the effects of high pressure on the optical spectroscopic properties of Ti^{2+}-doped NaCl. Most of the optical spectroscopic transition metal high-pressure studies published so far deal with ions, such as Cr^{3+} [28,46,47] or Mn^{2+},[31,48] neither of which is a dual emitter. Additionally, many of these studies were performed at room temperature, and consequently usually only broad and structureless luminescence features were observed. By studying Ti^{2+}:NaCl at 15 K the effect of pressure on excited-state distortions and force constants can be analyzed based on the vibrational fine structure present in its low-temperature luminescence bands.

After our previous brief reports on the title system and Ni^{2+}:$CsCdCl_3$,[12,13] this is the first detailed paper in which upconversion processes and properties are studied as a function of pressure. In Ti^{2+}:NaCl an efficient upconversion mechanism, which is inactive at ambient pressure, is switched on with pressure. Thus, pressure represents a valuable tool for the study of the various competing upconversion processes and mechanisms in transition metal upconversion systems. As such it can yield information which otherwise would only be accessible from a comparative optical spectroscopic study including a broad variety of chemically different upconversion systems.

Acknowledgment. The authors thank Rafael Valiente for valuable discussions. This work was supported by the Swiss National Science Foundation.

Supporting Information Available: Figure S1 presents the 15 K decays of the luminescence intensities from Figure 2 on semilogarithmic scales.This material is available free of charge via the Internet at http://pubs.acs.org.

References and Notes

(1) Jacobsen, S. M.; Güdel, H. U. *J. Lumin.* **1989**, *43*, 125.
(2) Wenger, O. S.; Güdel, H. U. *J. Phys. Chem. B* **2001**, *105*, 4181.
(3) Kasha, M. *Discuss. Faraday Soc.* **1950**, *9*, 14.
(4) Gamelin, D. R.; Güdel, H. U. *Topics in Current Chemistry*; Springer-Verlag: Berlin, 2000; Vol. 214.
(5) Gamelin, D. R.; Güdel, H. U. *Acc. Chem. Res.* **2000** *33*, 235.
(6) Auzel, F. E. *Proc. IEEE* **1973**, *61*, 758.
(7) Blasse, G.; Grabmaier, B. C. *Luminescent Materials*; Springer-Verlag, Berlin, 1994.
(8) See for example: Dalton, L. R.; Harper, A. W.; Goshn, R.; Steier, W. H.; Ziari, M.; Fetterman, H.; Shi, Y.; Mustacich, R. V.; Jen, A. K.-Y.; Shea, K. J. *Chem. Mater.* **1995**, *7*, 1060.
(9) Wenger, O. S.; Güdel, H. U. *Inorg. Chem.* **2001**, *40*, 5747.
(10) Wenger, O. S.; Gamelin, D. R.; Güdel, H. U. *J. Am. Chem. Soc.* **2000**, *122*, 7408.
(11) Wenger, O. S.; Güdel, H. U. *Inorg. Chem.* **2001**, *40*, 157.
(12) Wenger, O. S.; Valiente, R.; Güdel, H. U. *High-Pressure Research* **2002**, *22*, 57.
(13) Wenger, O. S.; Salley, G. M.; Valiente, R.; Güdel, H. U. *Phys. Rev. B* **2002**, *65*, 212108.
(14) Riesen, H.; Kindler, U.; Güdel, H. U. *Rev. Sci. Instrum.* **1987**, *58*, 1122.
(15) Piermarini, G. J.; Block, S.; Barnett, J. D.; Forman, R. A. *J. Appl. Phys.* **1975**, *46*, 2774.
(16) Ejder, J. *J. Opt. Soc. Am.* **1969**, *59*, 223.
(17) Lever, A. B. P. *Inorganic Electronic Spectroscopy*, 2nd ed.; Elsevier: Amsterdam, 1984.
(18) Sugano, S.; Tanabe, Y.; Kamimura, H. *Multiplets of Transition Metal Ions in Crystals*; Academic Press: New York, 1970.
(19) Ballhausen, C. J. *Introduction to Ligand Field Theory*; McGraw-Hill: New York, 1962.
(20) Figgis, B. *Introduction to Ligand Fields*; Interscience: New York, 1966; p 60.
(21) Jacobsen, S. M.; Güdel, H. U.; Daul, C. A. *J. Am. Chem. Soc.* **1988**, *110*, 7610.
(22) Jacobsen, S. M.; Smith, W. E.; Reber, C.; Güdel, H. U. *J. Chem. Phys.* **1986**, *84*, 5205.
(23) Bray, K. L. *Topics in Current Chemistry*; Springer-Verlag: Berlin, 2000; Vol. 213.
(24) Minomura, S.; Drickamer, H. G. *J. Chem. Phys.* **1961**, *35*, 903.
(25) See for example: Kittel, C. *Introduction to Solid-State Physics*, 7th ed.; Wiley: New York, 1996.
(26) Wallace, D. C. *Thermodynamics of Crystals*, John-Wiley: New York, 1972.
(27) Beggerov, G. In *Landolt-Börnstein Neue Serie IV, High-Pressure Properties of Matter*; Hellwege, K.-H., Ed.; Springer-Verlag: Berlin, 1980.
(28) Duclos, S. J.; Vohra, Y. K.; Ruoff, A. L. *Phys. Rev. B* **1990**, *41*, 5372.
(29) Rinzler, A. G.; Dolan, J. F.; Kappers, A.; Hamilton, D. S.; Bartram, R. H.; *J. Phys. Chem. Solids* **1993**, *54*, 89.
(30) Barriuso, M. T.; Aramburu, J. A.; Moreno, M. *Phys. Stat. Sol. B* **1996**, *196*, 193.
(31) Hernández, D.; Rodríguez, F.; Moreno, M.; Güdel, H. U. *Phys. B* **1999**, *265*, 186.
(32) Tutt, L.; Zink, J. I. *J. Am. Chem. Soc.* **1986**, *108*, 5830.
(33) Tutt, L. W.; Zink, J. I.; Heller, E. J. *Inorg. Chem.* **1987**, *26*, 2158.
(34) Wenger, O. S.; Valiente, R.; Güdel, H. U. *J. Chem. Phys.* **2001**, *115*, 3819.
(35) Sliwczuk, U.; Rinzler, A. G.; Kappers, L. A.; Bartram, R. H. *J. Phys. Chem. Solids* **1991**, *52*, 363.
(36) Brunold, T. C.; Güdel, H. U. *Inorganic Electronic Structure and Spectroscopy*; Solomon, E. I., Lever, A. B. P., Eds.; Wiley: New York, 1999; pp 259−306.
(37) Auzel, F. *C. R. Acad. Sci. Paris* **1960**, *262* 1016.
(38) For example, see: Valiente, R.; Wenger, O. S.; Güdel, H. U. *Phys. Rev. B* **2001**, *63*, 165102.
(39) Krämer, K. W.; Güdel, H. U.; Schwartz, R. N. *J. Alloys Compd.* **1998**, *275*−*277*, 191.
(40) Wermuth, M.; Riedener, T.; Güdel, H. U. *Phys. Rev. B* **1998**, *57*, 4369.
(41) Förster, Th. *Ann. Phys. (Leipzig)* **1948**, *2*, 55.
(42) Dexter, D. L. *J. Chem. Phys.* **1953**, *21*, 836.
(43) Pollnau, M.; Gamelin, D. R.; Lüthi, S. R.; Hehlen, M. P.; Güdel, H. U. *Phys. Rev. B* **2000**, *61*, 3337.
(44) Gamelin, D. R.; Güdel, H. U. *J. Phys. Chem. B* **2000**, *104*, 10222.
(45) Gamelin, D. R.; Güdel, H. U. *Inorg. Chem.* **1999**, *38*, 5154.
(46) Hömmerich, U.; Bray, K. L. *Phys. Rev. B* **1995**, *51*, 8595.
(47) Schäffer, C. E.; Lang, J. M.; Drickamer, H. G. *Inorg. Chem.* **1996**, *35*, 5072.
(48) Rodríguez, F.; Hernández, D.; Güdel, H. U. *Phys. Rev. B* **1999**, *60*, 10598.
(49) $\lambda_{exc} = 9500$ cm^{-1}, power: 50 mW.